Ultra-sharp plasmonic resonances from monopole optical nanoantenna phased arrays

Shi-Qiang Li,[1] Wei Zhou,[2] D. Bruce Buchholz,[1] John B. Ketterson,[3,4] Leonidas E. Ocola,[5] Kazuaki Sakoda,[4,6] and Robert P. H. Chang[1,4,a)]
[1]*Department of Materials Science and Engineering, Northwestern University, 2220 Campus Dr., Evanston, Illinois 60208-3108, USA*
[2]*Department of Chemistry and Chemical Biology, Harvard University, 12 Oxford St., Cambridge, Massachusetts 02138, USA*
[3]*Department of Physics, Northwestern University, 2145 Sheridan Rd., Evanston, Illinois 60208-3113, USA*
[4]*NU-NIMS Materials Innovation Center, 2220 Campus Dr., Evanston, Illinois 60208-3108, USA*
[5]*Center for Nanoscale Materials, Argonne National Laboratory, 9700 S Cass Ave., Lemont, Illinois 60439, USA*
[6]*National Institute for Materials Science, 1-2-1 Sengen, Tsukuba, Ibaraki 305-0047, Japan*

(Received 23 March 2014; accepted 4 April 2014; published online 9 June 2014)

Diffractively coupled plasmonic resonances possess both ultra-sharp linewidths and giant electric field enhancement around plasmonic nanostructures. They can be applied to create a new generation of sensors, detectors, and nano-optical devices. However, all current designs require stringent index-matching at the resonance condition that limits their applicability. Here, we propose and demonstrate that it is possible to relieve the index-matching requirement and to induce ultra-sharp plasmon resonances in an ordered vertically aligned optical nano-antenna phased array by transforming a dipole resonance to a monopole resonance with a mirror plane. Due to the mirror image effect, the monopole resonance not only retained the dipole features but also enhanced them. The engineered resonances strongly suppressed the radiative decay channel, resulting in a four-order of magnitude enhancement in local electric field and a Q-factor greater than 200. © *2014 AIP Publishing LLC*. [http://dx.doi.org/10.1063/1.4881323]

Resonant enhanced light-nanostructure interactions, particularly plasmonic resonances, have generated great scientific interest in recent years[1–4] in addition to opening new opportunities for sensing, imaging, and communications. The quality of an enhanced interaction is gauged by its field enhancement and resonance quality factor (Q, i.e., spectral width divided by spectral position).[5–8] To simultaneously achieve these properties is difficult. For example, augmented field enhancement is often accompanied by an increase of spectral width due to increased resistive losses.[9] Several recent studies revealed that high-Q modes with strong field-enhancement can be realized in plasmonic structures through strong coupling between a super-radiant mode (broad and bright) with a sub-radiant mode (narrow and dark).[10–13] Schatz *et al.*[14] and Markel[15] proposed a theory based on collective scattering and predicted that high-Q resonances will occur in periodic array of plasmonic spheres. Since then a series of experiments have demonstrated the observation of high-Q resonances.[16,17] In these studies, they identified that the challenge to observe and apply high-Q diffractively coupled plasmonic modes is two-fold: First, the study has been limited to planar 2-D periodic arrays, while it was known that controlling the third dimension is very critical to obtain optimized coupling and relaxes one more dimension of design space for tunability.[18] Second, the symmetry requirement for high-Q resonance has to be satisfied with index-matching. By doing so, the "hot spots" around the nano-structures are embedded in the index-matched matrix, thus rendering them difficult for many applications.[16,18–21]

To overcome these two barriers, we propose a method based on virtual image theory.[22] We show that ultra-sharp resonances can be engineered through diffractive coupling in a well-designed periodic vertically aligned indium tin oxide (ITO) nanorod arrays on a gold (or a perfect electric conductor, PEC) film. This arrangement gives the same resonant features and quality factor as in an array with twice the nanorod length in free space. This is because the gold/PEC film acts as a mirror plane, changes the dipole resonance of the free-standing nanorods to a monopole resonance, so that the symmetry is automatically satisfied, as shown in Fig. 1(a). The resulting resonances show giant electric field enhancement as well as the ultra-sharp line-widths of the resonances which were not observed with the 2-D planar cases with the long axes of nanorods lying in the array plane.[19,20,23]

Our study is focused on the interaction of longitudinal surface plasmon resonances (L-SPR, i.e., plasmon resonance along the long axis) from vertically aligned ITO nanorods with quasi-guided-modes (QGMs) within the plasmonic crystal slab,[24] analogous to the phased array in RF theory.[25] We start with optical simulations of 2-D freestanding nanorod arrays and arrays with half of the lengths on gold film or PEC boundary (Fig. 1). We chose 80° as the incident polar angle, so the wave-vector of the incident light is near parallel to the surface, which maximizes the electric field component along the nanorods and at the same time makes it possible for experimental measurements (see SI-3 in supplementary materials).[26] The resonant wavelength of L-SPR mode depends on the height as well as the spacing among the nanorods.[27,28]

a)Author to whom correspondence should be addressed. Electronic mail: r-chang@northwestern.edu

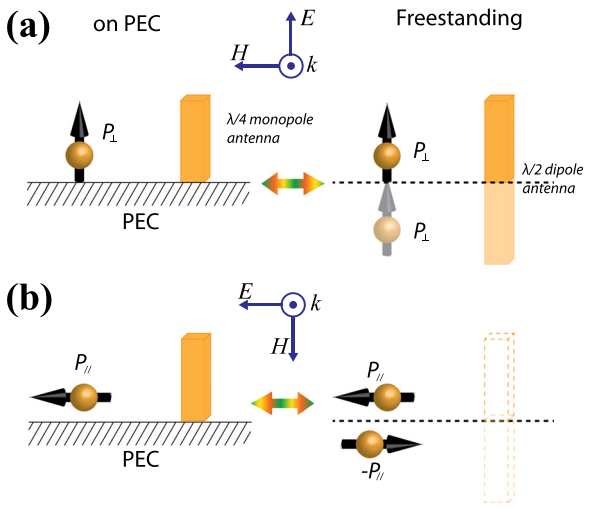

FIG. 1. The equivalency principle based on image theory. (a) shows the case of vertical electric dipole ($P_\perp$) sitting on top a PEC ground and a metal rod interacts with a plane wave, *p*-polarized with wavevector(k) parallel to the PEC ground plane. The optical response is equivalent to the cases shown on the right side, where the freestanding dipoles have their virtual images lying symmetrically with reflection at the symmetry plane (marked with dashed line). (b) shows the anti-symmetric behavior of horizontal dipole($P_{//}$) and a metal rod on PEC is equivalent to the freestanding case with anti-symmetric virtual images, resulting cancelled far-field optical responses. The direction of electric field is denoted as E and that of magnetic field is denoted as H.

These parameters can be optimized by simulation. It was found that under *p*-polarization, QGMs can indeed be effectively coupled to the L-SPR modes of ITO nanorods, resulting in strong narrow resonances. The calculated absorption spectra and the parameters of the array are shown in Fig. 2(a). We can see that all three cases (free-standing, on gold, and on PEC) show the same spectral features. The resonances are assigned according to the calculated dispersion diagram of guided modes (see SI-4 Figure S4)[26] in Fig. 2(a). The most interesting resonant position is the degenerated [1 ± 1] and [2 0] modes around $\lambda = 5\ \mu$m. Two other strong resonant positions are at [2 ± 1], $\lambda = 4\ \mu$m, and [3 0], $\lambda = 3.3\ \mu$m. Besides the sharp resonances assigned to the guided modes, a broad peak from 3 to 5 μm can be seen, which is associated with the L-SPR mode supported in individual nanorods. Due to the interaction of the QGMs with the broad L-SPR, the sharp resonances feature an asymmetric Fano lineshape.[29]

Experimentally, the direct measurement of absorption is difficult, so the far-field reflectance or transmittance measurement is usually the most straightforward way to probe the resonant modes supported by the plasmonic crystal slabs. In the case of arrays with a conductive substrate (or conductive film with thickness greater than the skin depth), the transmittance is negligible, therefore, most information can be obtained from the reflectance measurement. By comparisons between the reflectance spectra and the absorption spectra shown in Fig. 2, we can find the correspondences of different features. The broad reflectance minimum is the L-SPR peak in the absorption; the sharp dips/valleys are the QGMs with strong absorption, while the sharp increases of reflectance in the L-SPR hump are the modes with absorption minima. The reflectance from the free-standing array resembles the absorption spectrum and is relatively low, as they do not have a reflective surface underneath.

It was evident by a comparison between the features at 5 μm and 3.3 μm that the interference between the L-SPR mode and QGM has resulted in strong and narrow absorption peaks in one case but valleys/dips in the other. Interestingly, the peaks locate on the longer wavelength side of the L-SPR mode while the valleys locate on the shorter wavelength shoulder of the L-SPR absorption. This implies that the

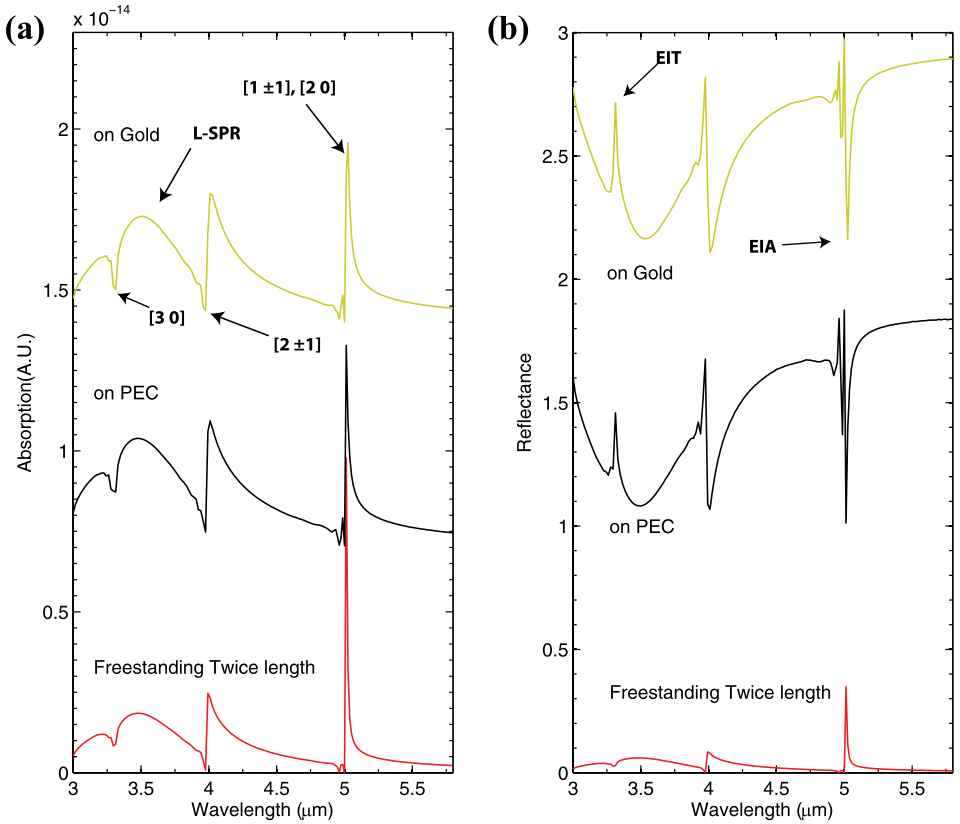

FIG. 2. (a) is the absorptions and (b) is the specular reflectance spectra of free-standing array, array on PEC, and gold calculated from FEM simulation. The curves are offset from each other by equal amount for clarity. The array is square lattice with 5 μm lattice constant formed by the basis consists of a rectangular ITO nanorod with 185 nm × 185 nm × 1000 nm side lengths, the permittivity of ITO was fitted with Drude Model (see SI-1).[26] The scattering plane is along one of the principal axes of the lattice, which means the azimuthal angle is zero (see SI-2).[26]

interferences at the peak positions are constructive (electromagnetically induced absorption or EIA) while the interferences at the valley positions are destructive (electromagnetically induced transparency or EIT), analogous to the same concepts in atomic physics.[30] These positions were marked in Fig. 2(b) and will be discussed later with coupled dipole model.

We examine the near field distribution from our simulations to understand these interferences instructively. In analogy to antennas in RF theory, array on gold film is like quarter-λ antenna array sitting on a mirror (as shown in Fig. 1(a)), we expect that the synthesized field pattern to be an overlap of the top half from the half-λ freestanding antenna array with its own bottom half, therefore, the field intensity will be about twice of the case of freestanding array.

We pick three representative spectral features to study. First, the narrow absorption feature at the vicinity of $\lambda = 5\,\mu$m is shown in Figs. 3(a) and 3(b) for half-λ freestanding nanorod array and quarter-λ nanorod array on gold, respectively. As we predicted, the enhancement around the nanorod in both cases are strong and similar to each other. The array on gold has stronger field due to the mirror image effect. The maximum field intensity enhancement is about 4 orders of magnitude of the background incident field intensity. Second, the near field profile of the spectral positions of the absorption dip, $\lambda = 4\,\mu$m, is plotted in Figures 3(c) and 3(d). We can see that in this case, the field is constructively interfering in between the nanorods, and forming standing-wave patterns. The highest enhancement of the electric field is less than 2 orders of magnitude. In the case of free-standing array, the standing-wave pattern is tilted, which is a result of the oblique incident angle, while in the case of array on gold, the standing-wave pattern is approximately symmetric, a result of the interference between incident and reflected optical fields from the gold "mirror" surface. Third, the near field profile of L-SPR absorption peak at 3.5 mm is plotted in Figs. 3(e) and 3(f). The field is highly enhanced at the vicinity of the nanorods. The residual field enhancement at the space between the nanorods is the result of partial interferences of incident wave and scattered wave as they are not far from the grating modes.

For all three spectral features, the array on gold resembles the field pattern of the free-standing case by overlapping the bottom half with the top half, thus the field enhancement is more significant than the latter case. The narrow absorption peaks have field enhancement which is one order of magnitude higher than that of the L-SPR peak. On the other hand, the narrow absorption dips have one order of magnitude lower. These results match well with the image theory and constructive/destructive interference explanation.

The QGMs observed are results of interference of the scattered wave from the nanorods with the incident wave. This interference can be understood from coupled dipole approach developed in the literature.[14,31] The extinction cross-section of the array is described by the following equation:

$$\sigma_e = \mathrm{Im}\left(\frac{4\pi k\alpha}{1-\alpha S}\right), \tag{1}$$

where k is the wavevector of the incident field, α is the polarizability (which exhibits a Lorentzian pole type of resonance, used to fit the L-SPR of individual nanorod), and S is the lattice summation of the contributions of the re-radiated field from all other nanorods in the array. The S parameter can be calculated analytically (see SI-5)[26] and we found that at the spectral position of each QGM, real part of S peaks and is always positive. On the other hand, the real part of α goes from negative to positive when it goes from the shorter wavelength side of the resonance to the longer wavelength side of the resonance. Therefore, the real part of the denominator of Eq. (1), (1-αS), can go across zero on the longer wavelength side of the resonance to maximize the extinction cross-section, while on the shorter wavelength side, $(1-\alpha S)$ is positive and large, thus peak values of S results a minimum of extinction cross-section. The calculated extinction curve agrees qualitatively with the experimental and simulation results (see SI-5 Figure S5).[26]

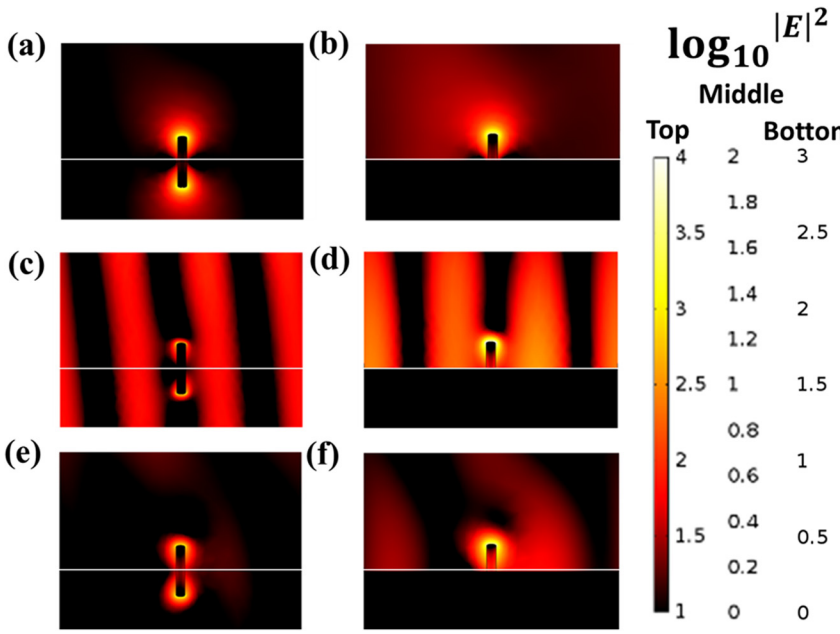

FIG. 3. The near field profiles at three representative spectral positions for free-standing array (Left column), array on gold (right column). The three representative spectral positions are the maximum absorption at the vicinity of 5 μm (top row), the minimum absorption at the vicinity of 4 μm (middle row), and the peak of the broad absorption (bottom row). Due to the significant difference of the near field profile, three different color map scales are used to show the features of the three different interference patterns, shown on the right side of the figure. The white lines in the near field profile plots mark the film surface in the cases of array sitting on gold, while they mark the half of the antenna length in the case of freestanding array.

We proceed to the experimental demonstration of the array on gold. Following the growth of ITO nanorod array,[28] a layer of 50 nm gold (>10 nm, which is the skin-depth of gold at the wavelength regime from 3 to 6 μm,) was coated to make sure that the mirror effect is valid. The scanning electron microscope (SEM) image of the array made is shown in Fig. 4(a). Owing to the gold coating, the plasma frequency used for ITO nanorod in the simulation (2.4 eV) is higher than the value normally reported (~2 eV), which is reasonable as the partial covering of gold at the surfaces of nanorods is equivalent to the increment of the plasma frequency of the nanorods (the evidence of partial gold coating can be seen from the SEM image presented in SI-6).[26]

The spectral peak positions and shapes from the experiments agree extremely well with simulations as shown in Figs. 4(b) and 4(c). It should be emphasized here that some of the peaks in the experimental results are extremely sensitive to the value of the azimuthal angle due to strong spatial dispersion of these delocalized modes, thus the source light needs to be highly collimated to obtain the sharp resonances. A comparison is made between the result obtained with focusing optics and the result from collimated source beam (see SI-7).[26] We found that the dispersion effect is stronger on modes which show larger angular dispersions. For example, [1 ± 1] and [2 ± 1] are varying rapidly with azimuthal angle, thus they are significantly broadened in the measured reflectance spectra (see Figures S2 and S5).[26]

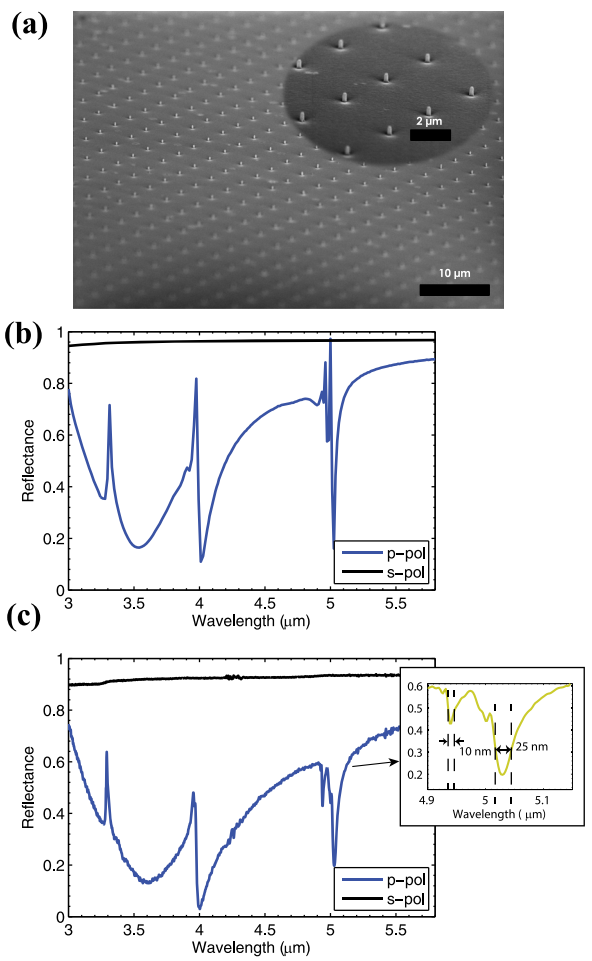

FIG. 4. (a) shows the scanning electron microscope image of the 5 μm × 5 μm square lattice ITO nanorod array and the inset is a zoom-in image of the same array. The nanorod measures with 185 nm side length and 500 nm height. The stage was tilted by 75° to reveal the 3rd dimension of the nanorod. (b) Simulation and (c) Experimental result of the coupling of quasi-guided modes with L-SPR mode. The lattice parameters used are square lattice with lattice constant of 5 μm. The peak positions match well and the magnitude matches qualitatively. It can be seen that with *s*-polarized light, the diffractive modes are inactive, so does the L-SPR mode, while strong resonances show in the spectra with *p*-polarized light. The black curves in (b) and (c) are the simulation and measurement results with the *s*-polarized light while keeping other parameters the same. The inset in (c) is a zoomed-in view of the narrow reflectance dips at around 5 μm observed on the ITO nanorod array on 50 nm gold film. FWHM of the side peak is about 10 nm and the main peak is about 25 nm.

The peak widths of our spectral features shown at around 5 μm have been measured in the inset of Fig. 4(c). The quality factors calculated are $Q_{tot} \sim 500$ for the side peak and $Q_{tot} \sim 200$ for the main peak, which supersedes the highest reported values in index-matched plasmonic systems.[32] The quality factor calculated from measurements matches exceedingly well with the simulation.

It is commonly understood that the quality factor is determined by radiative and non-radiative decay channels. In the system studied here, the super-radiant mode is the monopole plasmonic mode localized at individual optical antennas and the sub-radiant mode is the quasi-guided plasmonic mode delocalized in optical antenna arrays. The radiative component of damping can be extracted from simulation by artificially setting the imaginary part of the permittivity to zero for ITO nanorods,[33] from which we have obtained $Q_r = 5000$. Q_{tot} of the main peak is around 200. Based on the formula $Q_{tot}^{-1} = Q_{nr}^{-1} + Q_r^{-1}$, Q_{tot} is thus mainly determined by Q_{nr}, which is one order of magnitude lower than Q_r. This implies that the radiative decay for this resonance has been strongly suppressed, forcing a much slower dissipation of optical energy in the form of strong plasmonic oscillations, resulting high field enhancement and absorption. The high Q_{nr} comparing to a normal L-SPR is a result of the interference occurring at the edge of the antenna peak.

Another aspect of this system is the strong polarization dependence. In Fig. 4(c), plotted together with *p*-polarized reflectance curve is the reflectance curve from *s*-polarized light. The plot shows no spectral features and looks the same as the reflectance from the film without nanorods, as if the nanorods are "invisible" under *s*-polarized light. This has been explained by the image theory outlined in Fig. 1(b). As electric field with *s*-polarized light is parallel to the film surface, the effect of the gold film is equivalent as the generation of polarization along the opposite direction. Therefore, the summation of the dipole above and below the imaginary boundary results in the cancellation of the total dipole radiation field, leading to no far-field response from the array. Considering the filling fraction of nanorod scatterers is less than 0.1%, the optical response of this system with *p*-polarization is extremely strong.

A nanorod array sample was conformally coated with 60 nm zinc oxide film to study how this system responses to the change of environmental refractive index. As the mirror image effect makes sure that the symmetry requirement of sharp resonances will still be satisfied with coating, we expect that the peaks will remain narrow. Again, the measured reflectance matches extremely well with simulation, shown in Fig. 5. The peak resonance at 5 μm has shifted to 5.1 μm and broadened. Over 98% of the light has been absorbed at this peak resonance, implying almost perfect coupling of light to

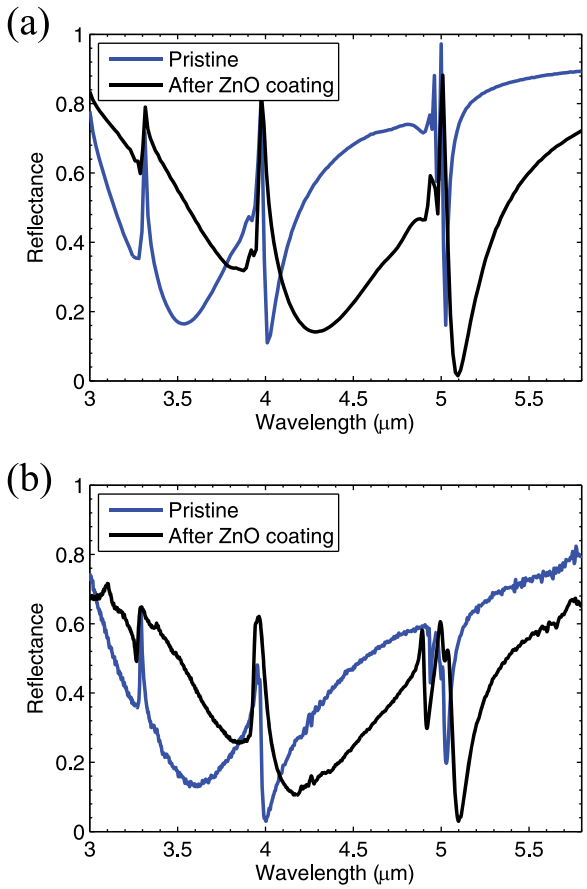

FIG. 5. The calculated and measured reflectance curves for the sample coated with 60 nm ZnO are presented in (a) and (b), respectively. In order to compare the results before coating, the reflectance curves from Fig. 4 are reproduced here as the blue curves.

the array. The broad L-SPR mode has also red-shifted significantly. For L-SPR and EIA at 5 μm, electric field is localized at the nanorod surface, thus the change of surface refractive index environments can strongly perturb the mode, which explains the significant red-shift of resonance features. The broadening of the peak resonance at 5.1 μm and the change of lineshape at 4 μm are results of the change of relative interference strength between L-SPR and guided mode. On the other hand, the peak positions of the interference peaks at 3.3 μm and 4 μm did not change, as the electric field has been delocalized from the nanorod by destructive interference, consistent with the near field profile in Figs. 2(c) and 2(d). The peak shape at 4 μm changed significantly due to the shift of LSPR peak from the left to the right side of the QGM.

In conclusion, we have proposed and demonstrated a monopole optical phased array, by transforming dipole resonance to monopole resonance with a mirror plane. This change has ensured that the symmetry required by coherent phase coupling is always satisfied, alleviating the need for index-matching. The resulting resonances from plasmonic-photonic coupling have ultra-sharp lineshapes. Furthermore, the coupling can be engineered to suppress the light-scattering efficiency by delocalizing the electric field creating EIT, or to strongly enhance the light scattering efficiency, resulting giant field enhancement and non-radiative decay (EIA). These findings suggest the proposed structure is extremely interesting for optical applications.

Supported by NSF funding (DMR-1121262 and DMR 0843962), QUEST computational resources (Project p20194 and Project p20447), and Center for Nanoscale Materials in Argonne National Laboratory (Project CNM 25883 and Project CNM 30831). Various characterizations were done in NUANCE center and KECK II Facilities in Northwestern University. The NUANCE Center and KECK II Facilities are supported by the NSF-NSEC, NSF-MRSEC, Keck Foundation, the State of Illinois, and Northwestern University. E-beam lithography was performed with JEOL-9300 in the Center for Nanoscale materials at Argonne National Laboratory. Use of the Center for Nanoscale Materials was supported by the U. S. Department of Energy, Office of Science, Office of Basic Energy Sciences, under Contract No. DE-AC02-06CH11357. S.Q.L. acknowledges Peijun Guo, Yi Hua, and Teri W. Odom for helpful discussions. The parameters for simulation and experiments are in the supplementary materials.

[1]P. Mühlschlegel, H.-J. Eisler, O. J. F. Martin, B. Hecht, and D. W. Pohl, Science **308**(5728), 1607 (2005).
[2]R. Stanley, Nat. Photonics **6**(7), 409 (2012).
[3]M. L. Brongersma, Nat. Photonics **2**(5), 270 (2008).
[4]D. K. Gramotnev and S. I. Bozhevolnyi, Nat. Photonics **4**, 83 (2010).
[5]S. Nie and S. R. Emory, Science **275**(5303), 1102 (1997).
[6]D.-K. Lim, K.-S. Jeon, H. M. Kim, J.-M. Nam, and Y. D. Suh, Nature Mater. **9**(1), 60 (2010).
[7]E. C. Le Ru and P. G. Etchegoin, Annu. Rev. Phys. Chem. **63**, 65 (2012).
[8]B. Min, E. Ostby, V. Sorger, E. Ulin-Avila, L. Yang, X. Zhang, and K. Vahala, Nature **457**(7228), 455 (2009).
[9]J. A. Schuller, E. S. Barnard, W. Cai, Y. C. Jun, J. S. White, and M. L. Brongersma, Nature Mater. **9**(3), 193 (2010).
[10]B. Luk'yanchuk, N. I. Zheludev, S. A. Maier, N. J. Halas, P. Nordlander, H. Giessen, and C. T. Chong, Nature Mater. **9**, 707 (2010).
[11]S. Zhang, D. A. Genov, Y. Wang, M. Liu, and X. Zhang, Phys. Rev. Lett. **101**(4), 47401 (2008).
[12]C. Wu, A. B. Khanikaev, R. Adato, N. Arju, A. A. Yanik, H. Altug, and G. Shvets, Nature Mater. **11**(1), 69 (2011).
[13]A. E. Miroshnichenko, S. Flach, and Y. S. Kivshar, Rev. Mod. Phys. **82**(3), 2257 (2010).
[14]S. Zou, N. Janel, and G. C. Schatz, J. Chem. Phys. **120**, 10871 (2004).
[15]V. A. Markel, J. Phys. B: At., Mol. Opt. Phys. **38**(7), L115 (2005).
[16]J. Sun, E. Timurdogan, A. Yaacobi, E. S. Hosseini, and M. R. Watts, Nature **493**(7431), 195 (2013).
[17]B. Auguié and W. L. Barnes, Phys. Rev. Lett. **101**(14), 143902 (2008).
[18]W. Zhou and T. W. Odom, Nat. Nanotechnol. **6**(7), 423 (2011).
[19]R. Adato, A. A. Yanik, C.-H. Wu, G. Shvets, and H. Altug, Opt. Express **18**(5), 4526 (2010).
[20]G. Vecchi, V. Giannini, and J. G. Rivas, Phys. Rev. B **80**(20), 201401 (2009).
[21]S. R. K. Rodriguez, A. Abass, B. Maes, O. T. A. Janssen, G. Vecchi, and J. Gómez Rivas, Phys. Rev. X **1**(2), 021019 (2011).
[22]J. D. Jackson, *Classical Electrodynamics*, 3rd ed. (Willey & Sons, New York, 1999).
[23]R. Adato and H. Altug, Nat. Commun. **4**, 2154 (2013).
[24]S. G. Tikhodeev, A. L. Yablonskii, E. A. Muljarov, N. A. Gippius, and T. Ishihara, Phys. Rev. B **66**(4), 045102 (2002).
[25]R. J. Mailloux, *Phased Array Antenna Handbook* (Artech House Boston, MA, 2005).
[26]See supplementary material at http://dx.doi.org/10.1063/1.4881323 for the details.
[27]L. Novotny, Phys. Rev. Lett. **98**(26), 266802 (2007).
[28]S. Q. Li, P. Guo, L. Zhang, W. Zhou, T. W. Odom, T. Seideman, J. B. Ketterson, and R. P. H. Chang, ACS Nano **5**(11), 9161 (2011).
[29]U. Fano, Phys. Rev. **124**(6), 1866 (1961).
[30]A. M. Akulshin, S. Barreiro, and A. Lezama, Phys. Rev. A **57**(4), 2996 (1998).
[31]V. A. Markel, J. Mod. Opt. **40**(11), 2281 (1993).
[32]A. A. Yanik, A. E. Cetin, M. Huang, A. Artar, S. H. Mousavi, A. Khanikaev, J. H. Connor, G. Shvets, and H. Altug, Proc. Natl. Acad. Sci. U. S. A. **108**(29), 11784 (2011).
[33]X. Yang, A. Ishikawa, X. Yin, and X. Zhang, ACS Nano **5**(4), 2831 (2011).